ELSEVIER

Journal of Nuclear Materials 290–293 (2001) 648–652

journal of nuclear materials

www.elsevier.nl/locate/jnucmat

# Heat load on the first wall materials and interaction of emitted neutrals with plasma

Kazuki Kobayashi [a,*], Shinichiro Kado [b], Bingjia Xiao [a], Satoru Tanaka [a]

[a] *Department of Quantum Engineering and Systems Science, School of Engineering, University of Tokyo, 7-3-1 Hongo, Bunkyo-ku, Tokyo, Japan*

[b] *High Temperature Plasma Center, University of Tokyo, 2-11-16 Yayoi, Bunkyo-ku, Tokyo, Japan*

**Abstract**

The relation between the interactions of $H_2$ with electron and plasma heat load to a tungsten target was investigated experimentally in the linear steady edge plasma simulator MAP-II. The heat load shows a large dependence on the density of injected $H_2$ gas ($N_{H_2}$), electron density ($n_e$) and electron temperature ($T_e$) in the region of interactions between $H_2$ and electrons. It was found that increase and decrease of the heat load can be described by characteristic lengths of several types of electron collisions normalized by the mean free paths of the corresponding collisions. In the plasma parameters surveyed in this work ($T_e$ of 5–20 eV and $n_e$ of $10^{16}$–$10^{18}/m^{-3}$), the increase of the heat load was mainly caused by the ionization of $H_2$ and the decrease was caused by the reduction of the electron energy through the interaction with $H_2$ and by the thermallization of the electrons through electron–electron collision. 

*Keywords:* Heat load; Ionization; Electron energy thermalization

## 1. Introduction

Hydrogen particles reflected or desorbed from the plasma facing materials have a large influence on the heat load to plasma facing materials. The heat load partially depends on the hydrogen reflection and thus the particle and energy reflection coefficient of the materials. The reduction of the heat load caused by ion reflection was observed experimentally in NAGDIS-I [1]. The impinging hydrogen particles which are not directly reflected from or permeate into the materials are desorbed as molecules except at high material temperature [2]. The desorbed $H_2$ affects largely the energy and particle balance in the edge plasmas through excitation, dissociation, ionization, charge exchange, etc. Experiments in TEXTOR [3] show that $H_2$ plays an important role in the energy exhaust mechanisms in divertor plasmas. Especially in the detached divertor regime, the radiation and the transport of the $H_2$ have a crucial role in the energy and particle balance in the edge plasmas, which dominates the initiation of the detachment in DIII-D [4], transport of impurities in JT60-U [5] and stability of the detached plasma [6]. Thus the behavior of the desorbed $H_2$ in the edge plasmas and the heat load are strongly related to each other. The desorbed $H_2$ interacts with the plasma in the vicinity of the target material. Thus the plasma parameters at the sheath edge vary sensitively. The heat transport through the sheath is largely affected by the plasma parameters at the sheath edge and also by the high energy electrons in the tail of the energy distribution, which determines the drop in the sheath potential. If the interaction scale length is shorter than the relaxation scale length of the electron temperature, the tail electrons easily reach to the target material without collision [7]. Indeed, non-maxwellian high energy electrons can be observed also in divertor region in tokamaks [8]. Therefore, the effect of desorbed $H_2$ on the heat load should be investigated in relation with the energy of the tail electrons.

It has been shown in our previous work that the heat load on C (Isotropic graphite) is higher than that on *W*

* Corresponding author.

*E-mail address:* kazuki@duke.q.t.u-tokyo.ac.jp (K. Kobayashi).

0022-3115/01/$ - see front matter 
PII: S0022-3115(00)00598-5

(tungsten) in hydrogen plasma discharge experiments in MAP-II [9]. The experimental results indicate that the higher heat load on C is caused by larger desorption and ionization rate of $H_2$. This cannot be explained by fluid models because the interaction length of $H_2$ and the electrons is shorter than the electron–electron collision mean free path. In this paper, we investigated experimentally the effect of the e–$H_2$ interactions on the heat load by puffing $H_2$ gas in the plasma near the *W* target. We considered the energy reduction of the tail electrons together with the excitation, dissociation, ionization of $H_2$ by the bulk electrons. We will discuss them analytically by the mean free path of each interaction.

## 2. Experiments

The cylindrical hydrogen plasmas are steadily generated in MAP-II (Fig. 1). Source gas is fed behind the $LaB_6$ cathode and the discharges are made between the cathode and the anode pipe. The plasmas are confined radially by a magnetic field of about 300 G and stopped at the *W*-test target plate in the target chamber. The *W* target is set on the water-cooled target holder and the potential of the target is kept floating. Hydrogen gas is puffed into the plasmas through an puffing nozzle set in the target chamber. The temperature increase of the target coolant is measured using thermocouples which are inserted into the coolant pipes of inlet and outlet. Electron density $n_e$ and electron temperature $T_e$ are measured using movable Langmuir probes set in the source chamber and the target chamber.

The *W* target was tested in nine discharge series in different conditions, namely, experiments 1–9, listed in Table 1. $H_2$ gas was puffed at different flow rates and the heat load at each flow rate was evaluated from the temperature increase of the target coolant. The discharge voltage, $V_d$, and the current, $I_d$, were kept at fixed values during the operations. In experiments 1–3, hydrogen gas puffing nozzle was placed close to the target surface to simulate the $H_2$ desorption from the C surface. While in experiments 4–9, it was placed at the bottom of the target chamber so that the density of puffed $H_2$ gas was supposed to be uniform in the plasma column due to large volume of the chamber ($\varnothing$ 50 cm × 50 cm). He, $H_2$ and mixtures of them were used as the plasma source gas aiming at controlling the $T_e$ and the $n_e$.

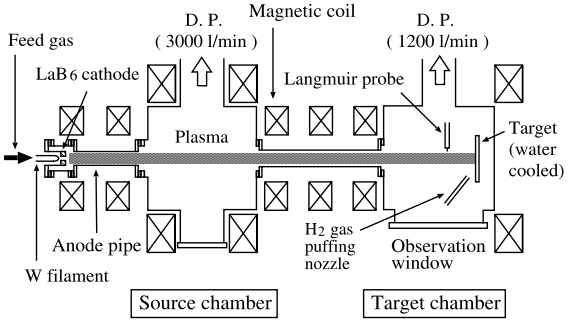


Fig. 1. Schematic diagram of linear steady edge plasma simulator MAP-II.

## 3. Results and discussion

Fig. 2 shows the time evolution of heat load measured by thermocouples of inlet and outlet in experiment 1. $H_2$ gas puffing was done at the target surface at the flow rate of 0.0, 0.016, 0.042 and 0.084 Pa $m^3$ $s^{-1}$ (at RT). Increase of the heat load with the gas puffing flow rate was clearly observed. We assume that this was caused by the interaction of puffed $H_2$ with the plasmas within the target chamber, because the space affected by the puffed $H_2$ is limited to the target chamber by the differential pumping: the increase of the $H_2$ pressure in the source chamber is less than 5% of that in the target chamber. Thus the effects of the puffing in the target chamber on $n_e$ and $T_e$ in the source chamber are small, and only the parameters in the target chamber are

Table 1
Experimental conditions

| Experiment | Plasma | $V_d$ (V), $I_d$ (A) | $H_2$ puffing flow rate ($10^{-2}$ Pa $m^3$ $s^{-1}$) | $n_e$ ($10^{18}$ $m^{-3}$) | $T_e$ (eV) |
|---|---|---|---|---|---|
| 1 | $H_2$ | 140, 16 | 0, 1.6, 4.2, 8.4 | 0.06 | 20 |
| 2 | $H_2$ | 120, 27 | 0, 1.6, 4.2, 8.4 | 1.3 | 15 |
| 3 | He | 80, 35 | 3.3, 4.9, 9.8, 16, 23 | 0.81 | 5.5 |
| 4 | $H_2$ | 105, 40 | 0, 4.2, 8.4 | 1.0 | 11 |
| 5 | $H_2$ | 110, 42 | 0, 4.2, 8.4 | 1.1 | 11 |
| 6 | He | 80, 40 | 0, 4.2, 8.4 | 1.1 | 7.6 |
| 7 | He | 90, 30 | 0, 4.2, 8.4 | 1.1 | 7.2 |
| 8 | $H_2$ (17%) He (83%) | 90, 40 | 0, 4.2, 8.4 | 0.94 | 8.4 |
| 9 | $H_2$ (30%) He (70%) | 100, 40 | 0, 4.2, 8.4 | 1.2 | 8.9 |

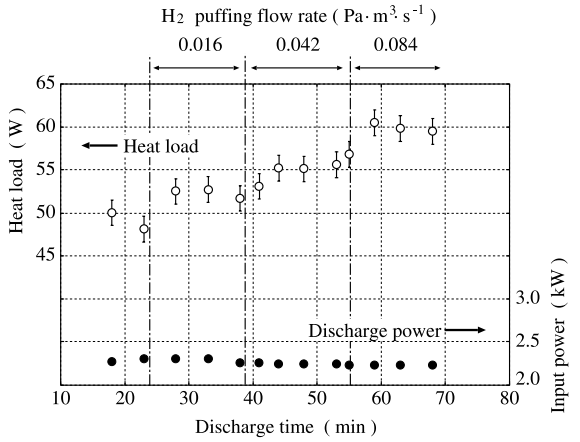


Fig. 2. Time evolution of measured heat load and discharge power in experiment 1.

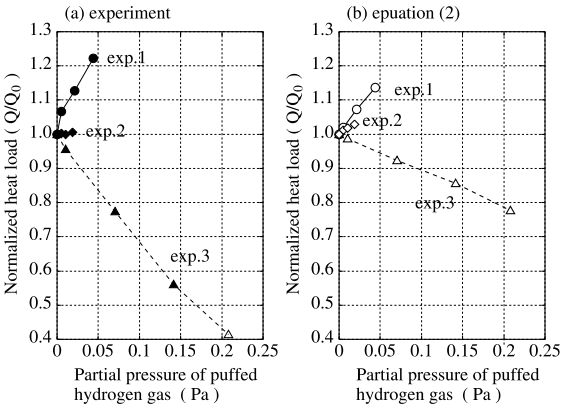


Fig. 4. Dependence of normalized heat load $Q/Q_0$ on $H_2$ puffing in experiments 1–3: (a) experimental results; (b) evaluated from Eq. (2).

modified (Fig. 3). Measured heat load in experiments 1–3 are reploted in Fig. 4(a). The $y$-axis is the heat load, $Q$, normalized to the heat load without $H_2$ puffing, $Q_0$, and the $x$-axis is the partial pressure of puffed $H_2$. The $n_e$ and the $T_e$ measured in the target chamber are also listed in Table 1. Listed $n_e$ and $T_e$ are mean values of that obtained upstream (40 cm from the target) and downstream (2 cm from the target). Errors of listed $n_e$ and $T_e$ are about 15%.

From Fig. 4 and Table 1, it seems that at higher $T_e$, the heat load increases or at higher $n_e$, the heat load decreases. This can be explained as follows. The heat load is mostly determined by the sheath potential which accelerates the ions and by the ion flux to the target. The sheath potential is formed by the high energy electrons in the tail of the velocity distribution. If the mean free path of e–e coulomb collision is shorter than the length of e–$H_2$ interaction region, the high energy electrons easily reach to the target without collision. Then the sheath potential does not decrease, while the ionization of $H_2$ occurs effectively by the bulk electrons and ion flux to the target increases. This leads to an increase of the heat load. In contrast, lower $T_e$ compared with threshold energy of $H_2$ ionization decreases the heat load because the reduction of the potential drop in the sheath becomes more effective than ionization of $H_2$. Higher $n_e$ also causes the heat load decrease because the reduction of the high energy electrons is enhanced by shorter e–e coulomb collision length, which leads to the reduction of the potential drop in the sheath. In this case the heat load is determined by the balance of e–e collision and e–$H_2$ collision in the interaction region. These situations can be fitted for our experimental conditions in this paper. This cannot be explained by a fluid model in which the electron energy distribution is treated as completely being thermallized.

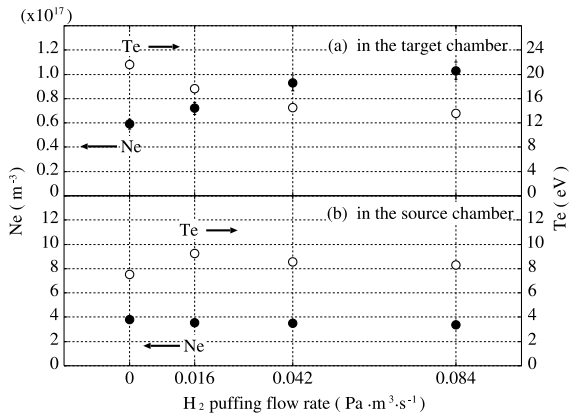


Fig. 3. Variation of $n_e$ and $T_e$ (center of the plasma column) by $H_2$ puffing: (a) in the target chamber; (b) in the source chamber.

To discuss the measured heat load analytically, we took into account the electron mean free path of e–e collision, $\lambda_{ee}$, $H_2$ ionization, $\lambda_i$ and non-elastic e–$H_2$ collisions, $\lambda_{coll}$. The reactions in each $\lambda$ having large rate coefficients [10] tabulated in Table 2 are considered in

Table 2
Reactions considered in $\lambda_i$ and $\lambda_{coll}$

| $\lambda$ | Reaction |
|---|---|
| $\lambda_i$ | (1) $e + H_2(X) \rightarrow e + H_2^+(v) + e'$ |
| | (2) $e + H_2(X) \rightarrow H_2^+(\Sigma_g, \Sigma_u) + e'$ |
| | $\rightarrow e + H^+ + H(1s) + e'$ |
| $\lambda_{coll}$ | (1) and (2) in $\lambda_i$ |
| | (3) $e + H_2(X) \rightarrow e + H_2^*(B)$ |
| | (4) $e + H_2(X) \rightarrow e + H_2^*(C)$ |
| | (5) $e + H_2(X) \rightarrow e + H_2^*(b, a, c)$ |
| | $\rightarrow e + H(1s) + H(1s)$ |
| | (6) $e + H_2(X) \rightarrow e + H_2^*(1s\sigma_g, nl\lambda|^1\Lambda)$ |
| | $\rightarrow e + H(1s) + H^*(2s)$ |

this paper. The $\lambda$s are described as $\lambda_{ee} = (3T_e/m_e)^{1/2}$ $((2\pi)^{1/2}6\pi\varepsilon_0^2 m_e^{1/2}T_e^{3/2})/(n_e e^4 \ln\Lambda)$, $\lambda_i = \bar{v}_e/(N_{H_2}\langle\sigma v\rangle_i)$ and $\lambda_{coll} = \bar{v}_e/(N_{H_2}\langle\sigma v\rangle_{coll})$, where $\bar{v}_e$ is the thermal velocity of electrons and $\ln\Lambda$ is the coulomb logarithm. The heat load must be characterized by the $\lambda$'s, with respect to the length of e–$H_2$ interaction region, $L_{H_2}$, which is defined by the length of the target chamber (50 cm) in our case. The heat flow to the target through the sheath can be described as

$$Q = -n_e C_s e\phi + 2kT_i n_e C_s + 2kT_e n_e C_s \times \left\{\left(1+\frac{T_i}{T_e}\right)\left(\frac{2\pi m_e}{m_i}\right)\right\}^{-1/2} \exp\left(\frac{e\phi}{kT_e}\right), \quad (1)$$

where $C_s$ is the ion sound speed and $\phi$ is the sheath potential [11]. In our case, the second term and the third term can be neglected because of small $T_i$ (<1 eV) and large $-e\phi/kT_e$ (3.5–4.0). Therefore, we considered that the heat load is proportional to $n_e$ and $-e\phi$. Considering that the $H_2$ is ionized by the electrons having the temperature $T_e$ in the target chamber, contribution of the ionization to the heat load can be written as $[1+\{1-\exp(-L_{H_2}/\lambda_i)\}]$. Decrease of $T_e$, namely the decrease of $-C_s e\phi$, can be expressed as the same manner like $[3/2T_e - \langle\epsilon\{1-\exp(-L_{H_2})/\lambda_{coll}\}\rangle]/(3/2T_e)$, where $\langle\epsilon\{1-\exp(-L_{H_2})/\lambda_{coll}\}\rangle$ is the mean energy loss of electron. In the case that the electrons cannot be thermallized within $L_{H_2}$, to describe the decrease of $-C_s e\phi$ by the reduction of the tail electrons, this value should be modified to a power $3/2\{1-\exp(-L_{H_2}/\lambda_{ee})\}$ which corresponds to the degree of the thermal equilibrium. Then, we describe the variation of the normalized heat load as

$$\frac{Q}{Q_0} = \left\{1+\left(1-e^{-(L_{H_2}/\lambda_i)}\right)\right\} \times \left\{\frac{(3/2)T_e - \langle\epsilon(1-e^{-(L_{H_2}/\lambda_{coll})})\rangle}{(3/2)T_e}\right\}^{(3/2)\left(1-e^{-(L_{H_2}/\lambda_{ee})}\right)}. \quad (2)$$

Using Eq. (2), we evaluated the variation of the heat load by the characteristic length of $-L_{H_2}/\lambda_i$, $-L_{H_2}/\lambda_{coll}$ and $-L_{H_2}/\lambda_{ee}$ obtained from the measured $n_e$, $T_e$ and $N_{H_2}$ in the corresponding experiments. We represent '$A$' for the first factor and '$B$' for the second factor in the right-hand side of Eq. (2). Fig. 4(b) shows the evaluated heat load. Although the absolute values deviate from the measured values in experiment 2 and experiment 3, dependence on the $H_2$ pressure is similar.

In experiments 1–3, the $H_2$ density is localized near the target because the puffing nozzle was placed at the target surface. It might cause ambiguity in $L_{H_2}$ and $N_{H_2}$. To avoid this, we made six other experiments (experiments 4–9), in which $H_2$ was puffed at the bottom of the target chamber. In this condition, the density of puffed $H_2$ is uniform in the target chamber and the error is reduced. The measured heat load for experiments 4–9 and evaluated values by Eq. (2) are plotted in Fig. 5. From the figure, the tendency of the heat load variation is well reproduced by Eq. (2). We can find that the tendency is not so much affected by the local density of $H_2$. The factor $A$ directly acts on the heat load in experiments 4–5 because the $B$ is almost unity. The contribution of the $B$ becomes stronger in experiment 6 and experiment 7 although $A > 1$. This indicates that the ionization of $H_2$ increases the heat load at higher $T_e$ or lower $n_e$. On the contrary, the effect of the reduction of the potential drop in the sheath overcomes the effect of the ionization at lower $T_e$ or higher $n_e$ and decreases the heat load. From these results, in case that the length of e–$H_2$ interaction region is shorter than that of e–e collision, we found that the tendency of the heat load variation can be explained by the characteristic length of $-L_{H_2}/\lambda_i$, $-L_{H_2}/\lambda_{coll}$ and $-L_{H_2}/\lambda_{ee}$.

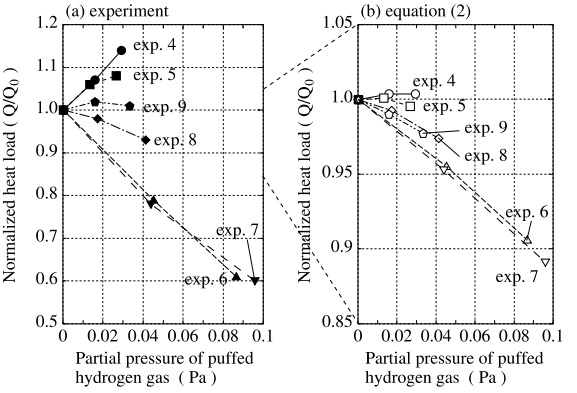


Fig. 5. Dependence of normalized heat load $Q/Q_0$ on $H_2$ puffing in experiments 4–5: (a) experimental results; (b) evaluated from Eq. (2).

One possibility for the deviation in absolute values is the fact that the effect of the vibrationally excited $H_2(H_2^*(v))$ is not taken into consideration. When the $H_2^*(v)$ exists, the threshold energies of ionization, excitation and dissociation are reduced and the variation of the factor $A$ and $B$ will be enhanced. Existence of $H_2^*(v)$ is reported from experiments in plasma devices [12,13]. The dissociated H atoms from $H_2^*(v)$ may also be considered because they can have significantly low energy ($\sim$0.3 eV). Such atoms have large possibility to interact with electrons and modify the estimation. Thus, the investigations of the vibrational states of $H_2^*(v)$ and the energy of H atoms by spectroscopic methods or numerical calculations are underway.

## 4. Conclusion

The relation between e–$H_2$ interactions and plasma heat load was investigated experimentally in MAP-II. It

was analyzed considering the electron's mean free paths of e–$H_2$ collision and e–e collision. We found that, when the length of e–$H_2$ interaction region is shorter than the e–e coulomb collision, the heat load can be described qualitatively by the characteristic length of $-L_{H_2}/\lambda_i$, $-L_{H_2}/\lambda_{coll}$ and $-L_{H_2}/\lambda_{ee}$.

## Acknowledgements

We wish to thank Professor T. Tanabe of Nagoya University for valuable discussions and advises on the experimental results. Further we acknowledge the technical advice about measurement system by Dr T. Yoneoka of University of Tokyo.

## References

[1] S. Masuzaki, J. Nucl. Mater. 223 (1995) 286.
[2] P. Franzen, E. Vietzke, J. Vac. Sci. Technol. A 12 (3) (1994) 820.
[3] A. Pospieszczyk, Ph. Mertens et al., J. Nucl. Mater. 266–269 (1999) 138.
[4] M.E. Fenstermacher, S.L. Allen et al., J. Nucl. Mater. 266–269 (1999) 348.
[5] K. Itami, N. Hosogane et al., J. Nucl. Mater. 266–269 (1999) 1097.
[6] S.I. Krasheninnikov, M. Rensink et al., J. Nucl. Mater. 266–269 (1999) 251.
[7] K. Kupfer, R.W. Harvey et al., Phys. Plasmas 3 (1996) 3644.
[8] J.G. Watkins, O. Batishchev et al., J. Nucl. Mater. (1996) 3644.
[9] K. Kobayashi, B. Xiao, S. Tanaka, Plasma Phys. Control. Fus., to be published.
[10] R.K. Janev, W.D. Langer et al., in: G. Echer et al. (Eds.), Elementary Processes in Hydrogen–Helium Plasmas, Springer, Berlin, 1987.
[11] P.C. Stangeby, in: D.E. Post, R. Behrisch, (Eds.), Physics of Plasma–Wall Interactions in Controlled Fusion, Plenum, New York, 1986, p. 41.
[12] U. Fantz, B. Heger, Plasma Phys. Control. Fus. 40 (1998) 2023.
[13] U. Fantz, K. Behringer et al., J. Nucl. Mater. 266–269 (1999) 490.